JACS
JOURNAL OF THE AMERICAN CHEMICAL SOCIETY
Article
pubs.acs.org/JACS

The Relationship between Threshold Voltage and Dipolar Character of Self-Assembled Monolayers in Organic Thin-Film Transistors

Michael Salinas,[†] Christof M. Jäger,[‡] Atefeh Y. Amin,[†] Pavlo O. Dral,[‡] Timo Meyer-Friedrichsen,[§] Andreas Hirsch,[⊥] Timothy Clark,[‡] and Marcus Halik*[,†]

[†]Organic Materials & Devices, Institute of Polymer Materials, University Erlangen-Nürnberg, Martensstraße 07, 91058 Erlangen, Germany

[‡]Computer Chemistry Center and Interdisciplinary Center for Molecular Materials, University Erlangen-Nürnberg, Nägelsbachstraße 25, 91052 Erlangen, Germany

[§]Heraeus Precious Metals GmbH & Co. KG, Conductive Polymers Division (Clevios), Chempark Leverkusen, Building B 202, 51368 Leverkusen, Germany

[⊥]Chair of Organic Chemistry II, University Erlangen-Nürnberg, Henkestraße 42, 91054 Erlangen, Germany

Supporting Information

ABSTRACT: We report a quantitative study that describes and correlates the threshold voltage of low-voltage organic field-effect transistors with the molecular structure of self-assembled monolayer dielectrics. We have observed that the component of the dipole moment of such self-assembled molecules perpendicular to the surface correlates linearly with the threshold voltage shift in devices. The model was validated using three different organic semiconductors (pentacene, α,α'-dihexylsexithiophene, and fullerene−C_{60}) on six different self-assembled monolayers. The correlation found can help optimize future devices, by tuning the dipole moments of the molecules that constitute the self-assembled monolayer.

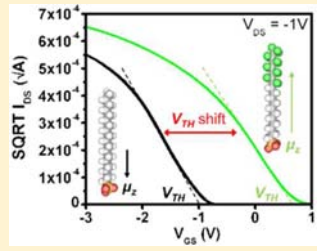

INTRODUCTION

Organic thin-film transistors (OTFTs) with hybrid nanodielectrics composed of thin oxide layers modified with a self-assembled monolayer (SAM) are promising devices for use in low-power integrated circuits (ICs).[1] Full control over the different transistor parameters (such as the threshold voltage, V_{TH}) of single transistors is essential for reliable operation of these integrated circuits.[2] In contrast to OTFTs, the origin of V_{TH} in silicon metal-oxide-semiconductor field-effect transistors is largely understood and has been described in the literature.[3] Control over the charge-carrier density in these devices is achieved by doping techniques such as ion implantation. In contrast, bulk and interface traps that are a consequence of the amorphous nature of the semiconductor and dielectric materials affect the charge carrier density in the semiconductor channel, and thus the device characteristics of thin-film transistors strongly.[3] In OTFTs, defects near the interface of semiconductor and dielectric contribute additional residual charge carriers in the conducting channel if not completely passivated by a proper surface treatment. Depositing densely packed SAMs on oxides has proven to be a reliable method for preventing undesired interactions between dielectric surface defects and the organic semiconductor, and thus for enhancing the OTFT performance. Well-formed SAMs on the oxide dielectric therefore reduce the gate leakage current and the impact of interfacial traps.[4] Moreover, several groups have addressed the control of charge-carrier densities in the semiconductor channel with SAMs by showing that the turn-on characteristics of a transistor are related to the dipole moment of the SAM-forming molecules. The mechanism relies on the formation of an electrostatic potential caused by the permanent dipoles of the molecules that make up the SAM. This potential can either generate mobile charge carriers in the semiconductor channel or withdraw them, depending on the direction of the dipole.[5] The relationship between the dipole moment of SAM molecules and the electrostatic potential drop across the molecular film is well understood and has been confirmed in several studies.[6−8] The predictive power of this relationship, however, could not be confirmed in attempts to quantify the effect of the dipole moment of SAM molecules on the threshold voltage of OTFTs.[9−12]

In this report we present a study of the correlation between the dipole moments of SAM-forming molecules and the threshold voltage of thin-film transistors with a hybrid gate dielectric composed of a thin aluminum oxide (AlO_x) layer and the corresponding SAM. We have investigated a set of functionalized *n*-alkane phosphonic acid (PA) molecules with different dipole moments (calculated using density-functional theory (DFT)) that were used to form self-assembled monolayers on an aluminum oxide dielectric. The deposition of PAs on AlO_x is known to yield high quality, densely packed SAMs.[1,13] We show that the shift of V_{TH} correlates linearly with the dipole moment component along the molecular axis for these transistors. This quantitative relationship was confirmed for the semiconductors α,ω-dihexylsexithiophene (DH6T), pentacene, and C_{60}.

Received: April 20, 2012
Published: June 26, 2012

dx.doi.org/10.1021/ja303807u | J. Am. Chem. Soc. 2012, 134, 12648−12652

EXPERIMENTAL SECTION

Device Fabrication. A schematic cross section of our bottom-gate top-contact transistors and the capacitor devices is shown in Figure 1.

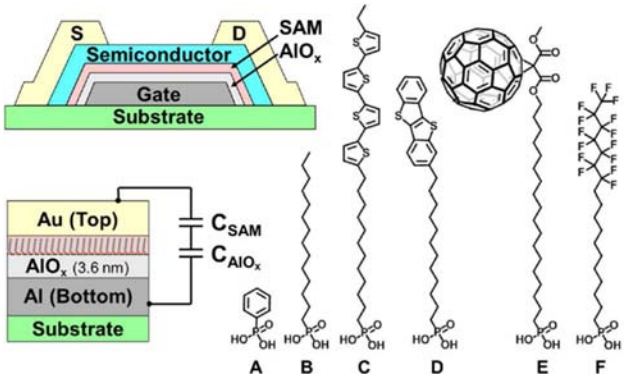

Figure 1. Layout of transistor and capacitor devices and molecules used for the formation of self-assembled monolayers (SAMs) on aluminum oxide.

The phosphonic acids used to form the SAMs are either commercially available or were synthesized as described in the references and are listed here according to the *z*-component of their dipole moment (μ_z). The *z*-direction is defined as that along the molecular axis for phenyl PA (**A**) and along the carbon chains of the stretched SAM molecules for tetradecyl PA (**B**), 12-(5‴-ethyl-2,2′:5′,2″:5″,2‴-quaterthien-5-yl)-dodecyl] PA (**C**),[14] 12-(benzo[*b*]benzo[4,5]thieno[2,3-d]thiophen-2-yl)dodecyl) PA (**D**),[15] [1-methoxy-3-(18-phosphonicacid octadecyloxy)-methano]-1,2-dihydro[60]fullerene (**E**),[16] and 12,12,13,13,14,14,15,15,16,16,17,17,18,18,18*H*-pentadecafluoro-octadecyl PA (**F**) (Figure 1).

The transistors were fabricated on a heavily p-doped silicon wafer with 100 nm thermally grown silicon dioxide using standard techniques.[17] A 30 nm layer of aluminum was first thermally evaporated through a shadow mask to form the gate electrode. The hybrid gate dielectric of aluminum oxide and SAM (AlO$_x$/SAM) was formed by oxygen plasma treatment and subsequent immersion into an approximately 0.1 millimolar solution of the SAM molecules in isopropyl alcohol for a minimum of 24 h. This procedure yielded densely packed self-assembled monolayers that were monitored by static contact angle and capacitance measurements. The organic semiconductors were deposited by thermal evaporation to create 30 nm polycrystalline films in all cases. The metal top electrodes (gold in the case of the p-type semiconductors and aluminum for C$_{60}$ samples) were thermally evaporated through a shadow mask to form fully patterned transistors with 40 μm channel length and 600 μm channel width. The capacitor stacks (MIM, metal/insulator/metal) with an area of 50 μm × 50 μm were fabricated on the same substrates simultaneously to the transistors.

Electrical Characterization. The capacitance was measured on samples with gold top electrodes (Al/AlO$_x$-SAM/Au) at a frequency of 100 kHz. The electrical characterization of the transistors was performed with a semiconductor parameter analyzer (Agilent 4156C) in a glovebox. All transfer scans were measured with an integration time of 50 ms, steps of 40 mV, and 2 s hold time and swept from positive to negative bias for p-type semiconductors and vice versa for C$_{60}$. The transistor parameters measured, threshold voltage V_{TH} and charge carrier mobility μ_{sat}, were determined by plotting the square root of the saturation current versus source−gate voltage as shown in Figure 2. Additionally, a backward threshold voltage ($V_{TH,back}$) was determined from the backward scan for SAMs that exhibit a notable hysteresis in the transfer scan analogously to V_{TH} in the forward scan. For such samples, the threshold voltage depends strongly on the starting bias applied in the transfer scan because of varying numbers of trapped charges induced by different biases. To rule out any effect of the measuring conditions on the threshold voltage, we kept the starting bias constant in the transfer measurements for each semiconductor (1 V for the p-type SCs and −0.5 V for C$_{60}$). The first measurement of each sample was always discarded and only fresh samples were used to avoid the known bias stress effect on the threshold voltage.[18]

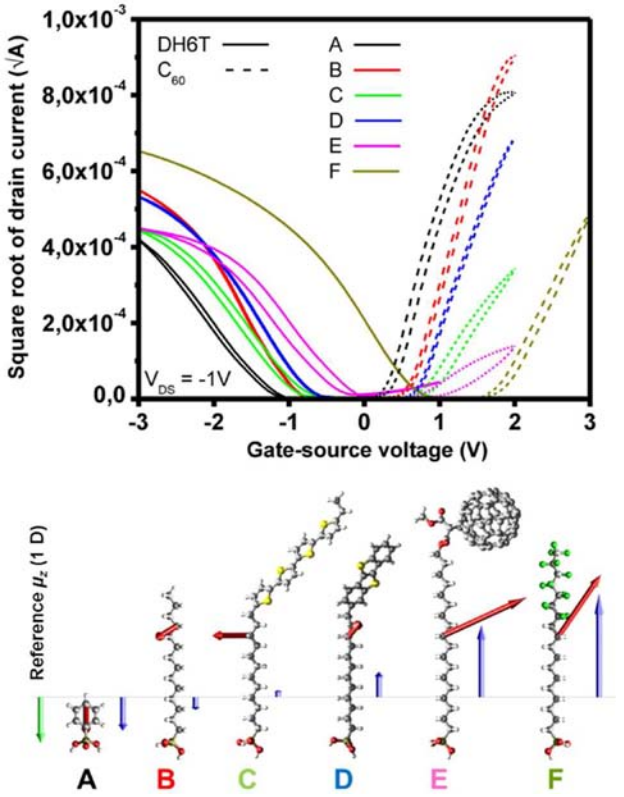

Figure 2. Representative transfer characteristics for OTFTs with DH6T and C$_{60}$ as semiconductors and different SAMs. (Bottom) The total dipole moments (in red) and the *z*-component of the dipole moment (in blue) are depicted together with a three-dimensional representation of the SAM molecules. The green reference arrow indicates the value of 1 D.

Computational Methods. The molecular dipoles were extracted from geometry-optimized structures of single molecules (**A**−**F**) using DFT calculations. The optimizations were carried out using the Perdew, Burke, and Ernzhof[19] functional (PBE) with the split valence basis set (SVP) from Schaefer, Horn, and Ahlrichs[20] and the SVPFit auxiliary basis.[21]

To estimate the work-functions of the different organic semiconductors, the band gaps were calculated from the lowest-energy excited states using the semiempirical UNO−CIS[22] method using the AM1 Hamiltonian.[23−27] Vertical and adiabatic electron affinities were calculated using different ab initio and DFT methods on geometries optimized at the PBEPBE/SVP/SVPFit level of theory. The results were compared to experimental values available for C$_{60}$ and pentacene, only. Details on the calculation of the work-functions are given in the Supporting Information.

UNO−CIS calculations were performed using the semiempirical MO program VAMP 11[28] and the DFT optimizations and electron affinity calculations with the Gaussian 09[29] program suite.

RESULTS AND DISCUSSION

Independently of the semiconductor, we observed a pronounced shift in V_{TH} from negative to more positive values with increasing dipole moment of the SAM molecules (Figure 2). The charge carrier mobilities ranged from 0.011 to 0.034 cm^2/(V s) for DH6T, 0.001 to 0.833 cm^2/(V s) for pentacene, and 0.004 to 0.164 cm^2/(V s) for C$_{60}$ (for complete list of values see Supporting Information). In all cases, the highest mobility was obtained for SAMs of molecule **B**. The mobility is known to

dx.doi.org/10.1021/ja303807u | J. Am. Chem. Soc. 2012, 134, 12648−12652

Table 1. Data Obtained for the *z*-Component of Dipole Moments (μ_z), Static Water Contact Angle (SCA) of the SAMs, Capacitance (C_i) of the Dielectric Stacks AlO_x/SAM, and Mean Threshold Voltage (V_{TH}) Measured for OTFT Devices in Saturation Regime

molecule	μ_z [D]	SCA [deg]	C_i [μF/cm^2]	DH6T V_{TH} ($V_{TH,back}$) [mV]	pentacene V_{TH} ($V_{TH,back}$) [mV]	C_{60} V_{TH} ($V_{TH,back}$) [mV]
ref	n/a[a]	<20	1.62	−660 ± 50	−970 ± 30	600 ± 30
A	0.721	70	1.44	−1100 ± 240	−1780 ± 70	310 ± 10
B	0.274	110	0.72	−860 ± 80	−1610 ± 50	330 ± 180
C	−0.149	80	0.72	−800 ± 140	−1370 ± 70	810 ± 70
				(−900 ± 120)	(−1460 ± 30)	(980 ± 150)
D	−0.561	80	0.82	−750 ± 20	−1230 ± 240	660 ± 40
E	−1.584	81	0.86	450 ± 40	−510 ± 70	830 ± 90
				(90 ± 30)	(−1090 ± 140)	(1120 ± 20)
F	−2.270	120	0.59	640 ± 10	−600 ± 40	1890 ± 120

[a]n/a = not applicable.

depend critically on factors such as surface energy match, grain size, and molecular order of the semiconductor.[10,30,31] The average values of V_{TH} for all SAMs and all semiconductors are listed in Table 1. Each value consists of measurements on at least four representative devices. Large values for hysteresis (>50 mV) were obtained for samples with SAMs of molecules **C** (thiophene-derivative) and **E** (fullerene-derivative), so that we also list $V_{TH,back}$ for these two molecules. V_{TH} values measured for reference transistors without SAM (also included in Table 1) were not considered for further evaluation. Without the SAM surface treatment after the oxygen plasma treatment reactive groups (e.g., hydroxyl groups) might lead to increased water absorption, making it impossible to control the surface composition and therefore also the electrostatic properties.

To relate the threshold voltage shift to the molecular structure of the SAM, we have plotted the measured values for V_{TH} and $V_{TH,back}$ as a function of μ_z (Figure 3). The black solid line

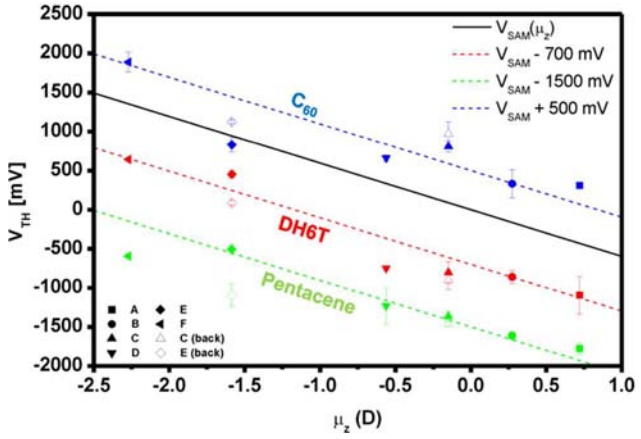

Figure 3. Mean values for V_{TH} plotted as a function of μ_z for different semiconductors. The solid black line indicates the theoretical correlation described by eq 1. Data for C_{60} is marked in blue, for DH6T in red, and for pentacene in green.

indicates the theoretical correlation between the electrostatic potential induced by the SAM dipole V_{SAM} and the dipole moment along the molecular axis μ_z, according to

$$V_{SAM} = \frac{N\mu_z}{\varepsilon_0 \varepsilon_{SAM}} \quad (1)$$

where N is the packing density and ε_{SAM} the relative permittivity of the SAM. We chose a value of 4.0×10^{14} cm^{-2} for N, assuming densely packed SAMs of all molecules. The theoretical maximum packing density of *n*-alkyl phosphonic acids (**B**) is 4.35×10^{14} cm^{-2}.[32] We expect a comparable packing density for most of the functionalized SAM molecules (**A**, **C**, **D**, and **F**) dictated by the footprint of the phosphonic acid anchor group. In the case of **E**, we expect a reduced packing density because of the large headgroup.[33] The relative permittivity of SAMs ε_{SAM} is typically low (e.g., our measured value of 2.4 for molecule **B** at 100 kHz). Consequently, we have obtained relative permittivities close to this value; from 2.1 for the fluorine containing molecule **F** to 3.7 for molecule **D**. We used a representative value of $\varepsilon_{SAM} = 2.5$ for the correlation shown in Figure 3. The choice of this value is arbitrary and impacts on the slope of the black solid line.

The theoretical description of $V_{SAM}(\mu_z)$ can be shifted vertically along the ordinate to match the data points for molecule **B**, indicated in dashed lines and different colors for each semiconductor. The trend suggested by the correlation between V_{SAM} and μ_z is supported fairly well by the data obtained for the other SAM-molecules, as predicted by eq 1. However, note that the surface potential shift calculated from eq 1 cannot be translated directly into a threshold voltage (or gate potential) shift as it is only related to the electric field induced in the SAM. To obtain the shift in the gate potential, the entire dielectric layer between gate electrode and semiconductor must be taken into account.

The number of charge carriers induced by the SAM (Q_{SAM}) is given by the product of the electrostatic potential induced by the SAM (V_{SAM}) and the capacitance of the SAM (C_{SAM}). To obtain the resulting shift of the gate voltage ($V_{TH,SAM}$), however, Q_{SAM} has to be related to the total capacitance of the dielectric stack. Hence, the gate potential shift induced by the SAM can be expressed by

$$\Delta V_{TH,SAM} = \frac{Q_{SAM}}{C_{total}} = \frac{C_{SAM}}{C_{total}} V_{SAM} \quad (2)$$

Similar relationships have been used in prior work to explain the threshold voltage or turn-on voltage shifts in SAM-modified OTFTs.[10,11]

Also note that, in case of a hybrid dielectric, which is composed of a thin AlO_x layer and the SAM in our transistors, two capacitors in series (AlO_x and SAM) are assumed.[5] Hence, the total capacitance can be obtained by the following relationship

$$\frac{1}{C_{total}} = \frac{1}{C_{AlO_x}} + \frac{1}{C_{SAM}} \quad (3)$$

dx.doi.org/10.1021/ja303807u | J. Am. Chem. Soc. 2012, 134, 12648−12652

Equation 3 implies that the total capacitance is dominated by the dielectric component with the lowest capacitance. For our transistor devices, the capacitances of all SAMs are considerably lower than that of the aluminum oxide layer (the theoretical capacitance of AlO_x is approximately 2.21 $\mu F/cm^2$, assuming a relative permittivity of 9 and a thickness of 3.6 nm[1]), leading to a quotient of C_{SAM}/C_{total} close to unity. For instance, the total capacitance C_{total} measured for the stack of AlO_x/**B** is 0.72 $\mu F/cm^2$. The theoretical capacitance C_{SAM} for a SAM of molecule **B** is approximately 1.1 $\mu F/cm^2$ calculated with $\varepsilon_B = 2.4$ and assuming a SAM thickness of 1.95 nm, which corresponds to the length of molecule **B**.[34] For molecule **F**, we measured a total capacitance C_{total} of 0.59 $\mu F/cm^2$ and calculated a theoretical capacitance C_{SAM} of 0.81 $\mu F/cm^2$ with $\varepsilon_F = 2.1$ and a SAM thickness of 2.3 nm.

In the case of thicker dielectrics modified with SAMs, the quotient C_{SAM}/C_{total} becomes quite large due to the decreased capacitance of the entire dielectric C_{total}. For SiO_2 dielectrics with a thickness of several hundred nanometers decorated with silanes, the potential shifts induced by the SAM can be enhanced considerably, leading to large V_{TH} shifts in the range of several tens of volts.[9,10] However, we cannot discard the possibility of space charge layers, residual charge carriers or trapped charges in the dielectric, introduced by charge transfer between the SAM or dielectric defects and the semiconductor, as general effects that affect the threshold voltage of SAM-modified transistors, as described by Possanner et al., Fleischli et al., and Gholamrezaie et al., respectively.[12,35,36] However, the fair agreement between the experimental data and the theoretical expectations leads us to conclude that these effects do not play a major role in our devices.

The shifts from the black solid line for the different semiconductors (Figure 3) may allow us to estimate additional contributions to the threshold voltage. For instance, the flat-band potential, which accounts for any work-function difference between semiconductor and the gate electrode, is known to contribute to the charge accumulation in the semiconductor.[3,37] We have related the work functions calculated for the three semiconductors to the deviations from the theoretical correlation given by eq 1. The work function WF of the semiconductors were estimated by

$$\mathrm{WF} = \chi + \frac{E_g}{2} \tag{4}$$

where χ is the electron affinity and E_g is the electronic band gap. The values obtained for the work functions (pentacene = 1.73 eV, DH6T = 2.08 eV, C_{60} = 3.29 eV) scale qualitatively with the order of the shifts (pentacene = −1500 mV, DH6T = −700 mV, C_{60} = 500 mV), and therefore support our assignment of the contribution of the flat-band potential to the measured threshold voltages. However, further contributions to the charge accumulation and therefore to the measured threshold voltage can originate from an ohmic drop through the semiconductor.[37] Polarization of the organic semiconductor at the metal electrodes can also play an important role for the charge injection into the organic semiconductor and can therefore impact V_{TH}.[38]

Thus, the dipole effect cannot be defined exactly as several additional effects related to the properties of the SAM molecules and the SAM morphology also contribute to the absolute values of V_{TH}. Charge trapping affects the threshold voltage, as has been extensively reviewed by Dhar et al.[39] If charge trapping is involved, it is difficult to relate the measured values for V_{TH} with the properties of the dielectric layer unless the number of trapped charges is known. The absolute V_{TH} values have to be corrected further for fixed oxide charges. However, as the formation of the AlO_x layer was performed identically for each sample, this contribution can be assumed to be constant for all devices.

Furthermore, functionalized molecules such as **B** and **E** can form semiconducting channels in SAMFETs.[14] In these cases, the SAM molecules can interact with the overlying semiconductor and contribute to charge transport at the interface, therefore reducing the effective dipole of the SAM. These two contributions might explain the small deviations of data points obtained for molecules **B** and **D** combined with DH6T and molecule **E** combined with C_{60}.

The thin-film growth of the semiconductor on the SAM cannot only affect the mobility, but also the threshold voltage if it results in an incomplete layer with gaps. Such is the case for pentacene grown on SAMs of molecule **F** (see Figure 4), which is

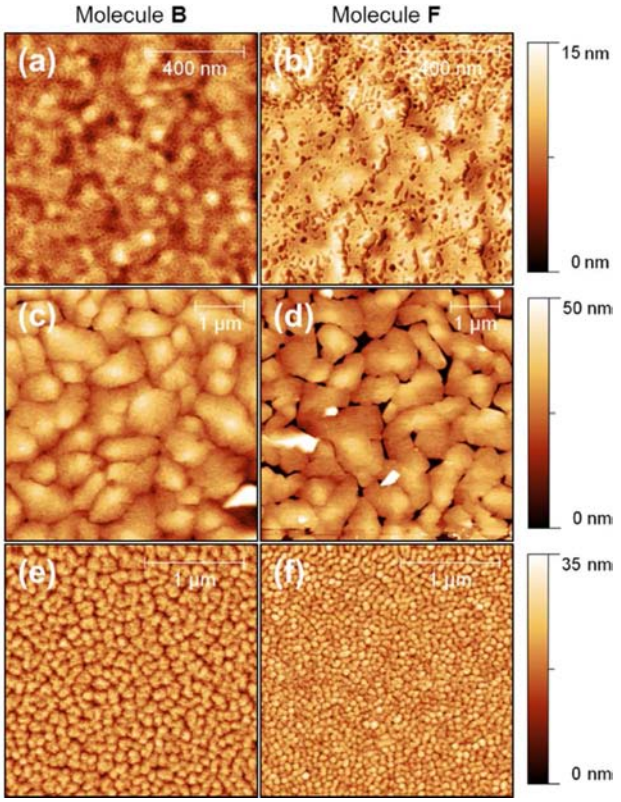

Figure 4. Morphology of DH6T (a and b), pentacene (c and d), and C_{60} (e and f) on SAMs of molecules **B** and **F**, respectively. The layer of 30 nm pentacene on molecule **F** exhibits large gaps in contrast to all other SAM-SC combinations.

known to exhibit low surface energy (approximately 9 mN/m) and thus lead to three-dimensional island growth with edge-on oriented molecules.[31] The reduced area of the interface between semiconductor and dielectric requires a higher electric field to accumulate the same number of charges as in a complete layer (e.g., pentacene on molecule **A**), therefore leading to a shift of V_{TH} to more negative bias.

CONCLUSIONS

In summary, our results provide a general approach to tuning the threshold voltage of organic thin-film transistors with dipolar monolayers and even for predicting V_{TH}-values from the *z*-component of the molecular dipole of the SAM molecules. We found that theoretical predictions regarding the impact of

dx.doi.org/10.1021/ja303807u | J. Am. Chem. Soc. 2012, 134, 12648−12652

molecular modifications of organic electronic materials and even whole devices can be used for self-assembled monolayers that serve as a part of the gate dielectric in OTFTs. An exact prediction of absolute threshold voltage values, however, requires specific properties of organic materials, such as redox properties or thin-film growth behavior, and their impact on the transistor parameters to be considered.

■ ASSOCIATED CONTENT

Supporting Information

Complete list of measured charge carrier mobilities and details on the calculation of the work functions. This material is available free of charge via the Internet at http://pubs.acs.org.

■ AUTHOR INFORMATION

Corresponding Author

marcus.halik@ww.uni-erlangen.de

Notes

The authors declare no competing financial interest.

■ ACKNOWLEDGMENTS

The authors gratefully acknowledge the funding of the German Research Council (DFG), HA 2952/4-1, the Collaborative Research Center 953 and the "Excellence Initiative" supporting the Cluster of Excellence "Engineering of Advanced Materials" (www.eam.uni-erlangen.de), and the Erlangen Graduate School of Molecular Science (GSMS).

■ REFERENCES

(1) Klauk, H.; Zschieschang, U.; Pflaum, J.; Halik, M. *Nature* **2007**, *445*, 745−748.
(2) Zschieschang, U.; Ante, F.; Schlorholz, M.; Schmidt, M.; Kern, K.; Klauk, H. *Adv. Mater.* **2010**, *22*, 4489−4493.
(3) Sze, S. M. *Physics of Semiconductor Devices*, 3rd ed.; John Wiley & Sons, Inc.: New York, 2007.
(4) Halik, M.; Klauk, H.; Zschieschang, U.; Schmid, G.; Dehm, C.; Schutz, M.; Maisch, S.; Effenberger, F.; Brunnbauer, M.; Stellacci, F. *Nature* **2004**, *431*, 963−966.
(5) Chung, Y.; Verploegen, E.; Vailionis, A.; Sun, Y.; Nishi, Y.; Murmann, B.; Bao, Z. *Nano Lett.* **2011**, *11*, 1161−1165.
(6) Bruening, M.; Cohen, R.; Guillemoles, J. F.; Moav, T.; Libman, J.; Shanzer, A.; Cahen, D. *J. Am. Chem. Soc.* **1997**, *119*, 5720−5728.
(7) Ashkenasy, G.; Cahen, D.; Cohen, R.; Shanzer, A.; Vilan, A. *Acc. Chem. Res.* **2002**, *35*, 121−128.
(8) Cahen, D.; Naaman, R.; Vager, Z. *Adv. Funct. Mater.* **2005**, *15*, 1571−1578.
(9) Kobayashi, S.; Nishikawa, T.; Takenobu, T.; Mori, S.; Shimoda, T.; Mitani, T.; Shimotani, H.; Yoshimoto, N.; Ogawa, S.; Iwasa, Y. *Nat. Mater.* **2004**, *3*, 317−22.
(10) Pernstich, K. P.; Haas, S.; Oberhoff, D.; Goldmann, C.; Gundlach, D. J.; Batlogg, B.; Rashid, A. N.; Schitter, G. *J. Appl. Phys.* **2004**, *96*, 6431.
(11) Huang, C.; Katz, H. E.; West, J. E. *Langmuir* **2007**, *23*, 13223−13231.
(12) Fleischli, F. D.; Suarez, S.; Schaer, M.; Zuppiroli, L. *Langmuir* **2010**, *26*, 15044−15949.
(13) Ma, H.; Acton, O.; Ting, G.; Ka, J. W.; Yip, H.-L.; Tucker, N.; Schofield, R.; Jen, A. K. Y. *Appl. Phys. Lett.* **2008**, *92*, 113303.
(14) Novak, M.; Ebel, A.; Meyer-Friedrichsen, T.; Jedaa, A.; Vieweg, B. F.; Yang, G.; Voitchovsky, K.; Stellacci, F.; Spiecker, E.; Hirsch, A.; Halik, M. *Nano Lett.* **2011**, *11*, 156−159.
(15) Meyer-Friedrichsen, T.; Reuter, K.; Elschner, A.; Halik, M. WIPO International Patent 2011, WO 2012/010292 A1.
(16) Burkhardt, M.; Jedaa, A.; Novak, M.; Ebel, A.; Voitchovsky, K.; Stellacci, F.; Hirsch, A.; Halik, M. *Adv. Mater.* **2010**, *22*, 2525−2528.
(17) Jedaa, A.; Halik, M. *Appl. Phys. Lett.* **2009**, *95*, 103309.
(18) Zschieschang, U.; Weitz, R. T.; Kern, K.; Klauk, H. *Appl. Phys. A, Mater.* **2009**, *95*, 139−145.
(19) Perdew, J. P.; Burke, K.; Ernzerhof, M. *Phys. Rev. Lett.* **1996**, *77*, 3865−3868.
(20) Schafer, A.; Horn, H.; Ahlrichs, R. *J. Chem. Phys.* **1992**, *97*, 2571−2577.
(21) Eichkorn, K.; Treutler, O.; Ohm, H.; Haser, M.; Ahlrichs, R. *Chem. Phys. Lett.* **1995**, *242*, 652−660.
(22) Dral, P. O.; Clark, T. *J. Phys. Chem. A* **2011**, *115*, 11303−11312.
(23) Dewar, M. J. S.; Thiel, W. *J. Am. Chem. Soc.* **1977**, *99*, 4899−4907.
(24) Dewar, M. J. S.; McKee, M. L.; Rzepa, H. S. *J. Am. Chem. Soc.* **1978**, *100*, 3607−3607.
(25) Dewar, M. J. S.; Zoebisch, E. G.; Healy, E. F.; Stewart, J. J. P. *J. Am. Chem. Soc.* **1985**, *107*, 3902−3909.
(26) Dewar, M. J. S.; Reynolds, C. H. *J. Mol. Struct.: THEOCHEM* **1986**, *136*, 209−214.
(27) Davis, L. P.; Guidry, R. M.; Williams, J. R.; Dewar, M. J. S.; Rzepa, H. S. *J. Comput. Chem.* **1981**, *2*, 433−445.
(28) Clark, T.; Alex, A.; Beck, B.; Burkhardt, F.; Chandrasekhar, J.; Gedeck, P.; Horn, A.; Hutter, M.; Martin, B.; Dral, P. O.; Rauhut, G.; Sauer, W.; Schindler, T.; Steinke, T. *VAMP 11.0*; University of Erlangen: Germany, 2011.
(29) Frisch, M. J. T., G., W.; Schlegel, H. B.; Scuseria, G. E.; Robb, M. A.; Cheeseman, J. R.; Scalmani, G.; Barone, V.; Mennucci, B.; Petersson, G. A.; Nakatsuji, H.; Caricato, M.; Li, X.; Hratchian, H. P.; Izmaylov, A. F.; Bloino, J.; Zheng, G.; Sonnenberg, J. L.; Hada, M.; Ehara, M.; Toyota, K.; Fukuda, R.; Hasegawa, J.; Ishida, M.; Nakajima, T.; Honda, Y.; Kitao, O.; Nakai, H.; Vreven, T.; Montgomery, Jr., J. A.; Peralta, J. E.; Ogliaro, F.; Bearpark, M.; Heyd, J. J.; Brothers, E.; Kudin, K. N.; Staroverov, V. N.; Kobayashi, R.; Normand, J.; Raghavachari, K.; Rendell, A.; Burant, J. C.; Iyengar, S. S.; Tomasi, J.; Cossi, M.; Rega, N.; Millam, N. J.; Klene, M.; Knox, J. E.; Cross, J. B.; Bakken, V.; Adamo, C.; Jaramillo, J.; Gomperts, R.; Stratmann, R. E.; Yazyev, O.; Austin, A. J.; Cammi, R.; Pomelli, C.; Ochterski, J. W.; Martin, R. L.; Morokuma, K.; Zakrzewski, V. G.; Voth, G. A.; Salvador, P.; Dannenberg, J. J.; Dapprich, S.; Daniels, A. D.; Farkas, Ö.; Foresman, J. B.; Ortiz, J. V.; Cioslowski, J.; Fox, D. J. *Gaussian 09*, revision A.02; Gaussian, Inc.: Wallingford, CT, 2009.
(30) Knipp, D.; Street, R. A.; Völkel, A.; Ho, J. *J. Appl. Phys.* **2003**, *93*, 347.
(31) Novak, M.; Schmaltz, T.; Faber, H.; Halik, M. *Appl. Phys. Lett.* **2011**, *98*, 093302.
(32) Luschtinetz, R.; Oliveira, Augusto F.; Duarte, Hélio A.; Seifert, G. *Z. Anorg. Allg. Chem.* **2010**, *636*, 1506−1512.
(33) Rumpel, A.; Novak, M.; Walter, J.; Braunschweig, B.; Halik, M.; Peukert, W. *Langmuir* **2011**, *27*, 15016−15023.
(34) Jedaa, A.; Burkhardt, M.; Zschieschang, U.; Klauk, H.; Habich, D.; Schmid, G.; Halik, M. *Org. Electron.* **2009**, *10*, 1442−1447.
(35) Possanner, S. K.; Zojer, K.; Pacher, P.; Zojer, E.; Schürrer, F. *Adv. Funct. Mater.* **2009**, *19*, 958−967.
(36) Gholamrezaie, F.; Andringa, A. M.; Roelofs, W. S.; Neuhold, A.; Kemerink, M.; Blom, P. W.; de Leeuw, D. M. *Small* **2011**, 8.
(37) Horowitz, G.; Hajlaoui, R.; Bouchriha, H.; Bourguiga, R.; Hajlaoui, M. *Adv. Mater.* **1998**, *10*, 923.
(38) Amy, F.; Chan, C.; Kahn, A. *Org. Electron.* **2005**, *6*, 85−91.
(39) Dhar, B. M.; Özgün, R.; Dawidczyk, T.; Andreou, A.; Katz, H. E. *Mater. Sci. Eng. R* **2011**, *72*, 49−80.